https://doi.org/10.5194/egusphere-2024-3222
Preprint. Discussion started: 20 November 2024

Measurement Report: Influence of particle density on secondary ice production by graupel and ice pellet collisions

Sudha Yadav[1], Lilly Metten[1], Pierre Grzegorczyk[2], Alexander Theis[3], Subir K. Mitra[3], and Miklós Szakáll[1]

[1]Institute for Atmospheric Physics, Johannes Gutenberg University, Mainz, Germany
[2]Laboratoire de Météorologie Physique (UMR6016)/UCA/CNRS, Aubière, France
[3]Particle Chemistry Department, Max Planck Institute for Chemistry, Mainz, Germany,

Correspondence: Miklós Szakáll (szakall@uni-mainz.de)

Abstract. We present a laboratory study dedicated to fragmentation due to graupel-graupel and ice pellet-ice pellet collisions and their role in augmenting ice particle concentration in clouds. For this, graupels of different sizes and densities were created utilizing dry growth condition in a cold chamber at -7 °C and -15 °C using a setup that simulates the natural rotation and tumbling motion of freely falling graupels. Ice pellets were generated by freezing water in 3D-printed spherical molds. We conducted collision experiments inside the cold chamber utilizing a fall tube that ensures central and repeatable collision of ice particles at different collision kinetic energies. The number of fragments generated in the collisions were analyzed following a theoretical framework as a function of the collision kinetic energy. Our results revealed a strong dependency of the fragment number on the density of the colliding ice particles, which can be attributed to the particles' structure. The number of fragments varies between 1 and 20 and, thus, comparable or larger than those resulted in drop freezing experiments. The size of the fragments was in the sub-mm range for graupels, and up to 3 mm for ice pellets. Another set of experiments, focusing on multiple collision of graupel revealed that the number of fragments generated becomes zero when the particle suffers more than three collisions in a row.

1 Introduction

Ice particles are generated in the atmosphere either by primary processes like homogeneous freezing or heterogeneous ice nucleation from the liquid or vapor phase, or by secondary ice processes (SIP), which is the generation of ice crystals during processes that involve already existing ice particles. There is a consent that SIP (also known as ice multiplication) is responsible for the observed discrepancy between the number of detected ice crystals and ice nucleation particles (INPs) in the atmosphere (Field et al., 2017; Korolev et al., 2022). In spite of their crucial importance, the basic understanding of SIP is still lacking due to the scarcity of systematic laboratory studies (Korolev and Leisner, 2020). Currently, seven different mechanisms are distinguished as possible SIP processes. The most prominent for decades, has been the rime splintering (also known as Hallett-

https://doi.org/10.5194/egusphere-2024-3222
Preprint. Discussion started: 20 November 2024

Mossop, hereinafter abbreviated as H-M process) in which ice splinters are produced upon accretion of ~ 20-μm-sized droplets by ice particles between $-3\,^{\circ}\mathrm{C}$ and $-8\,^{\circ}\mathrm{C}$ (e.g. Hallett and Mossop, 1974; Mossop, 1976; Choularton et al., 1978, 1980; Heymsfield and Mossop, 1984). However, the relevance of this process in the atmosphere became debated recently. Seidel et al. (2024) conducted rime-splintering experiments under H-M conditions and detected no ice crystal formation. The second promising SIP process is the fragmentation during freezing (Lauber et al., 2018; Keinert et al., 2020). Lauber et al. (2018) distinguished between ice particle ejection and splitting during drop freezing. Although the number of the generated secondary ice particles is strongly drop-size dependent, it can exceed unity (~ 2.4), especially bubble bursting might be very productive. Further SIP, like ice fragmentation due to sublimation (Oraltay and Hallett, 1989), due to activation of INPs in transient supersaturation (Prbhakaran et al., 2020), due to thermal shock (Dye and Hobbs, 1968), and during break-up of freezing droplets on impact of ice particles (James et al., 2021) have been supported experimentally but remained uncharacterized yet.

In a recent study (Grzegorczyk et al. (2023b); hereinafter G2023), we investigated fragmentation due to collision of ice particles, which was in some sense a follow-up experiment of earlier investigations of Takahashi et al. (1995) and Vardiman (1978). Motivated by the analysis of the dendritic growth zone by long-term radar observations of von Terzi et al. (2022), the collision of snowflake proxies were studied. For that, we used graupel particles with dendritic crystals grown on their surface, and natural-like snowflakes produced from dendritic crystals grown in an aquarium setup. Our G2023 study revealed that hundreds of ice fragments can be generated when particles with dendritic crystal structures are breaking apart upon collision. The fragment numbers were characterized in terms of the collision kinetic energy (CKE), which is defined as

$$CKE = \frac{1}{2}\frac{m_1 m_2}{m_1 + m_2}(\Delta v)^2 \tag{1}$$

where m_1 and m_2 are the masses of the colliding particles, and Δv is their fall velocity difference.

Phillips et al. (2017) (hereinafter P2017) introduced a full physical formulation of mechanical breakup of ice particles due to collision, which is based on an energy conservation principle. In this theoretical framework, the number of fragments N generated by collision is calculated as

$$N = \alpha A\left(1 - \exp\left(-\left[\frac{C \cdot CKE}{\alpha A}\right]^{\gamma}\right)\right) \tag{2}$$

where α is the surface area of the smaller colliding particle; A is the number of breakable asperities per unit area; while C is the asperity-fragility coefficient, which is an inverse measure of the average work to break each branch or other asperity. Both A and C are dependent on the morphology of the more fragile particle in the collision, thus, on temperature, maximum dimension, rime fraction, and particle type (i.e. graupel, snow, or hail). In G2023 and in its corrigendum we provided the parameters A, C, and γ for graupels with dendrites on their surface, bare graupels, and snowflakes.

Nevertheless, ice-ice collisions might also be important if there are no dendritic crystals grown on their surface. This is the case, when graupel particles and ice pellets are formed in a relatively small and well-defined region inside clouds, like in the embryo growth zone of thunderstorm clouds, for instance. Furthermore, when graupels are generated in mixed phase clouds, they might collide due to their abundance, although the collision rate is presumably less than in thunderstorm clouds. Griggs and Choularton (1986) pointed out that the strength of rime decreases as the temperature is lowered. Moreover, in an

https://doi.org/10.5194/egusphere-2024-3222
Preprint. Discussion started: 20 November 2024

underestimated environment, sublimation would further weaken the structure making the rimed graupel more fragile. They concluded that vapor grown crystals would produce more fragments than rime. Another important aspect to mention is, that if the concentration of graupels or ice pellets is high, they might collide multiple times, which enhances the ice multiplication mechanism. The collision process between graupels or between ice pellets can be significant over a relatively large temperature range from -3 to -20 °C, i.e. including also the H-M temperature conditions.

This paper aims to investigate the fragmentation of bare graupels and ice pellets due to collision, and extends our earlier investigation with graupels having dendritic crystals grown on their surface. The investigation of the collision of bare graupels and ice pellets also enables the study of the effect of particle morphology or structure on the fragmentation outcome.

2 Experimental

The experimental studies were performed inside the walk-in chamber of the Mainz vertical wind tunnel laboratory. Graupel and ice pellet generation and collisions were carried out at -5 °C, -7 °C and -15 °C. These temperatures correspond to regions where rimed particles are observed in mixed-phase clouds (Waitz et al., 2022). Furthermore riming can also occur at even lower temperatures, (e.g. down to -20 °C; see in Tridon et al., 2022). The graupel particles generated at -7 °C and -15 °C (as in G2023) possess different morphological structures and, therefore, different densities. This is because supercooled droplets freeze faster at lower temperatures than at higher, leading to more air inclusion into the graupel structure, making its density less (Enzmann et al., 2011).

2.1 Graupel generation

Rimed lump graupels were generated using the graupel generator GEORG, which is described in G2023 in detail and originally introduced in Theis et al. (2022). The graupel generation is performed inside a 2-m-high flow tube having a cross-sectional area of 17 cm $\times$ 17 cm. A small epoxy sphere acts as an ice embryo which is exposed to a supercooled droplet stream, and the graupel grows by riming. Droplets with diameters of 19.7 $\pm$ 5.1 μm (modal), 23.4 $\pm$ 8.8 μm (arithmetic mean), and 34.6 $\pm$ 9.9μm (volume) are produced by an ultrasonic atomizer (US 2/58 Hz, Lechler GmbH, Germany) using a 30 L/min nitrogen flux, and injected to form a central droplet stream inside the flow tube. A blower is mounted at the top of the equipment and ensures a flow speed of 2.78 $\pm$ 0.10 m/s to simulate graupel free fall. The liquid water content (LWC) for typical graupel conditions was 0.368 $\pm$ 0.028 g/m^3 which establishes dry growth conditions. To minimize the effect of turbulence inside GEORG, which was very likely responsible for a relatively large number of graupel with unwanted size or density during the preparation phase of our former experiments in G2023, a honeycomb structure was placed at the bottom of GEORG, from where the air is sucked in. The setup can simulate the falling and tumbling motion of a graupel in natural clouds by a double gyration motor apparatus to which the graupel is attached. This apparatus consists of one motor rotating around the vertical axis at 4 Hz, and a second one fixed at 45° angle with respect to the first one and rotating at the same rotational speed.

For the present experiments we generated graupels at -7 °C having an average diameter of 2.45 $\pm$ 0.28 mm and a density of 0.558 $\pm$ 0.02 gcm-3 . In the experiments of G2023, graupels were 2.48 $\pm$ 0.17 mm, 2.12 $\pm$ 0.1 mm, and 4.0 $\pm$ 0.2 mm in

https://doi.org/10.5194/egusphere-2024-3222
Preprint. Discussion started: 20 November 2024

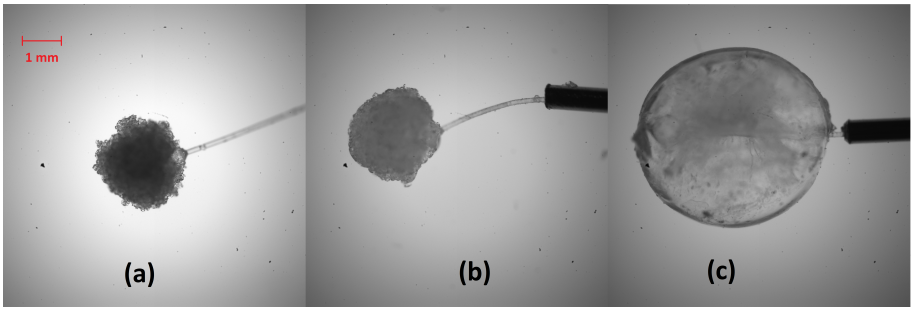

Figure 1. Microscope images of graupels with (a) a diameter of 2.23 mm and a density of 0.334 g cm^{-3}, grown at -15 °C and 0.723 g m^{-3} LWC for 10 minutes in G2023; (b) a diameter of 2.4 mm and a density of 0.558 g cm^{-3}, grown at -7 °C and 0.368 g m^{-3} LWC for 5 minutes in the present study; and (c) an ice pellet of 5 mm diameter. The red bar indicates 1 mm.

diameter with densities of 0.21 $\pm$ 0.05 g cm^{-3}, 0.334 $\pm$ 0.062 g cm^{-3} and 0.51 $\pm$ 0.07 g cm^{-3}. The low density of 0.21 g cm^{-3} was achieved by growing dendritic crystals on the surface of the graupel particle (see G2023 for details). Furthermore, the G2023 experiments were conducted at -15 °C. Images of graupels generated for the current measurements as well as in G2023 are depicted in Fig. 1a and b.

2.2 Generation of ice pellets

Ice pellets were generated by freezing Milli-Q water in a 3D-printed spherical mold inside a deep freezer at -70 °C. Before the collision experiments, the mold was kept at the cold room temperature of either -5 °C or -15 °C for several minutes, then briefly held and warmed in both palms to facilitate its easy removal. The ice pellets used in the collision experiments were 5 mm (shown in Fig. 1c.) and 7 mm in diameter, and had densities of 0.89 $\pm$ 0.02 g cm^{-3}, i.e. corresponding to atmospheric small hail densities (Lachapelle and Thériault, 2022). The different experimental temperatures enabled a systematic study into the effect of any temperature and structural variation of ice on fragmentation.

3 Collision experiments and fragment analysis

The collision experiments were carried out using the same setup as in G2023 (see their Fig. 6) which consists of a "collision tube" and a "fall tube". One particle is kept stagnant in the collision tube using a thin plastic wire fitted into a cannula. The wire is flexible and possesses a small aerodynamic resistance, therefore, the particle can freely move after collision. Hence, the collision energy is not consumed by the mounting and fed only into the kinetic energies of the colliding particles and into fragmentation, which we could prove by high-speed video recordings. The 8-mm-thin fall tube guides the falling particle to the impact point and ensures a central collision between the two particles. In the bare graupel collision experiments we abandoned placing the aquarium underneath the collision setup as in G2023, because the sublimation of the graupel particles was negligible.

https://doi.org/10.5194/egusphere-2024-3222
Preprint. Discussion started: 20 November 2024

One aim of the present study was to derive a relationship between CKE and the number of fragments generated. Therefore, collisions with different CKEs but same particle types and masses were carried out. For that, the falling particle was released from different heights of 5 cm, 22 cm, and 80 cm. For each particle type and size, and for each fall height the particles' velocities were determined from high speed (2000 frames-per-seconds) images recorded in a characterization set of measurements. The masses and sizes of the graupel particles were also measured during the characterization measurements after producing several particles in GEORG under predefined conditions, like temperature, growth time, LWC. In case of ice pellets, masses of several frozen spheres of 5 mm and 7 mm in diameter were measured and averaged. Densities were calculated from particle mass and size. Since we observed that the epoxy inside a falling graupel modified the center of mass of the particle, and therefore one fall orientation was preferred, we removed the epoxy from the falling graupel particle before the collision experiments. Thus, the density of the falling graupel became less than that of the fixed one.

To investigate the effect of a graupel experiencing random multiple collisions with other ice particles in the cloud, we conducted experiments where a 2.45-mm graupel and a 5-mm ice particle were collided up to six times. The multiple collision experiments were performed between graupel and ice sphere at the highest CKE, i.e. at a fall height of 80 cm, in order to account for the maximum possible number of fragments that are produced. The number of collision repetitions was determined based on the observation that after a certain number of collisions, no new fragments were produced, regardless of further collisions. For each subsequent collisions, a new graupel was used as the falling particle. The fall tube ensured that the falling particles hit the fixed one approximately at the same position.

In total, we conducted 15 series of experiments as listed in Table 1. Each series of experiments consisted of at least three individual collisions. The colliding particles were either ice pellets and ice pellets (II), graupels and graupels (GG), or graupels and ice pellets (GI). Particle sizes, densities, and the corresponding CKEs for each experimental series can be taken from Table 1. CKEs for graupels and ice pellets match the atmospheric values of these sizes when calculating the fall velocities using, e.g., the parameterization in Heymsfield et al. (2020), although they represent the highest end of the possible natural collision kinetic energies.

The ice fragments generated by collision were collected into a petri dish, which was filled with food grade mineral oil (density equal to 0.78 g cm^{-3} at room temperature) and placed at the bottom of the collision tube. The ice crystals were then analyzed under a microscope. In the case of multiple collisions, the petri dish was immediately removed after the collection of fragments during each collision and the images were analysed at the end of the experiment. For all collisions, total number of fragments, as well as fragment sizes were determined following the procedure described in G2023. We note here that the number of fragments was low for all collision types, therefore, it was not possible to provide any fragment size distribution from this study. Instead, we will provide the minimum and maximum fragment sizes found for each collisions. The size resolution of the applied optical setup was 3.8 μm-per-pixel. Nevertheless, we could not prevent the oil bath from being contaminated by dust particles (see Fig. 8b in G2023). This results in a detection limit for our analysis of 25 to 30 μm. Ice fragments larger than this size could be identified as ice particles with high reliability. However, this means also that any ice particles which were smaller than approximately 20 μm could not be distinguished from dust particles, thus, could not be detected.

https://doi.org/10.5194/egusphere-2024-3222
Preprint. Discussion started: 20 November 2024

Table 1. Main characteristics of the collision experiments. GG: graupel-graupel collisions, II: ice pellet – ice pellet collisions, GI: graupel-ice pellet collisions, MC: multiple collisions.

Exp#	Collision type	Temperature (°C)	Fixed particle		Falling particle		Fall height (cm)	CKE (μJ)
			Size (mm)	Density (g/cm^3)	Size (mm)	Density (g/cm^3)		
1	II	-5	5.00	0.89	7.00	0.89	22	65.35
2	II		5.00	0.89	7.00	0.89	80	267.46
3	II		5.00	0.89	5.00	0.89	22	71.92
4	II		5.00	0.89	5.00	0.89	80	203.79
5	II	-15	5.00	0.89	7.00	0.89	22	65.35
6	II		5.00	0.89	7.00	0.89	80	267.46
7	II		5.00	0.89	5.00	0.89	22	71.92
8	II		5.00	0.89	5.00	0.89	80	203.79
9	GG	-7	2.45	0.558	2.45	0.46	5	0.95
10	GG		2.45	0.558	2.45	0.46	22	3.15
11	GG		2.45	0.558	2.45	0.46	80	7.70
12	GI		2.45	0.558	5.00	0.89	5	1.96
13	GI		2.45	0.558	5.00	0.89	22	15.37
14	GI		2.45	0.558	5.00	0.89	80	27.13
15	MC		2.45	0.558	5.00	0.89	80	27.13

4 Results and discussion

4.1 Number of fragments after collision

Figure 2 shows the variation in the average number of fragments generated during the collisions as a function of the collision kinetic energy. The ice pellet – ice pellet collisions are presented in blue in Fig. 2a, whereas graupel–graupel and graupel–ice pellet collisions are shown in green in Fig. 2b. The average number of fragments released in each series of experiments are also provided in Table 2 together with their maximum and minimum values.

As expected, in both series of collisions the average number of fragments were observed to increase with increasing CKE. The data were fitted with the parameterization given in Eq. 2 and are represented by blue and green dashed lines in Fig. 2. The shaded areas in the two plots represent a 1σ standard deviation interval of the best fit curves. For fitting, the shape parameter γ was held constant at 0.78, which was also derived in G2023 for graupel–graupel with dendrites and graupel-snowflake collisions. Fitting the other parameters provided the values $A = 30610\ \mathrm{m}^{-2}$ and $C = 26534.5\ \mathrm{J}^{-1}$ for ice pellet – ice pellet, and $A = 126168\ \mathrm{m}^{-2}$ and $C = 150597\ \mathrm{J}^{-1}$ for graupel–graupel collisions.

Ice pellet–ice pellet collisions were conducted at two different temperatures, namely at -15 °C (shown with filled symbols in Fig. 1a) and at -5 °C (open symbols). There seems to be a temperature dependency of the number of fragments, and it is

https://doi.org/10.5194/egusphere-2024-3222
Preprint. Discussion started: 20 November 2024

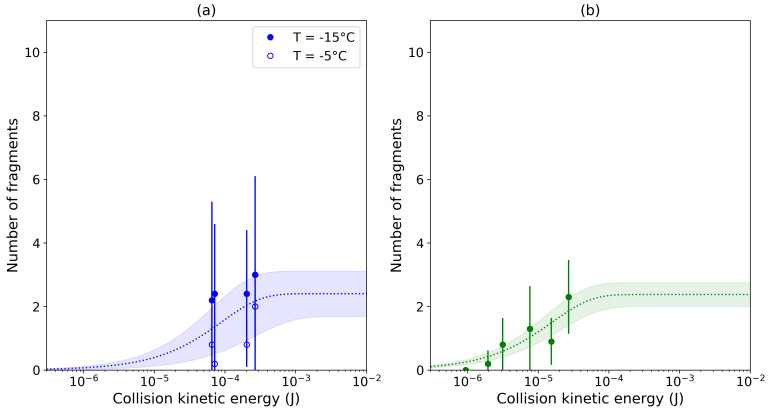

Figure 2. Number of fragments generated as a function of CKE during (a) ice pellet–ice pellet collisions at -5 °C and -15 °C (Exp# 1-8); and (b) during graupel–graupel and graupel–ice pellet collisions at -7 °C (Exp# 9-14). The dashed lines represent fits on data using Eq. 2, while the shaded areas are the 1σ standard deviation intervals of the fits.

by trend higher at lower temperature in the investigated temperature range (see also Table 2). This temperature dependency is similar to that found by (Takahashi et al., 1995). Nevertheless, the difference between the number of fragments at these two temperatures is within the error of the experiments. Therefore, we combined the two dataset for further discussion.

The minimum and maximum sizes of fragments produced are also listed in Table 2. Fragments during graupel-graupel collisions have a minimum size of 0.02 mm and a maximum size of 0.24 mm, whereas graupel–ice pellet collisions produced fragments with 0.02 mm minimum and 1.12 mm maximum sizes. In the case of collisions between ice pellets, there were not more than 3 fragments on an average (see Table 2), with fragments having a maximum average size of 1.2 mm and a minimum average size of 0.27 mm. For these ice pellet—ice pellet collisions there seems to be a slight tendency of particle size on CKE. The minimum sizes are comparable to the ice crystal maximum dimensions in G2023, but there are very large fragments within the maximum observed sizes for these collisions. This can most probably be attributed due to the high CKEs.

4.2 Compilation of the current results with G2023

Figure 3 depicts a composite plot of the current results together with the bare graupel – bare graupel collisions in G2023. For the G2023 plot, all collisions are taken into account, while for the current results an averaging over the collisions for each CKE are shown. The dashed lines represent the best fits using Eq. 2. For the sake of consistency, we employed the same shape parameter $\gamma = 0.78$ for the G2023 bare graupel data points as for the current graupel – graupel and ice sphere – ice sphere data. G2023 found the best fit on the data if the shape parameter was 0.78 for graupel-snowflake and graupel – graupel with dendrites collisions, while for bare graupel-bare graupel collisions $\gamma = 0.55$ was revealed as the best fit. Nevertheless, when we set γ to 0.78, it modified somewhat the curve but this change was insignificant and well within the measurement error. From Fig. 3, it is obvious that the average fragment number as a function of CKE is dependent on the particle density. The fragment number

https://doi.org/10.5194/egusphere-2024-3222
Preprint. Discussion started: 20 November 2024

Table 2. Average, minimum and maximum number of fragments, and minimum and maximum fragment sizes produced in each series of experiments. Collision type and temperature are also indicated.

Exp#	Collision type	Temperature (°C)	Frag. number mean (min;max)	Frag. size (mm) min	Frag. size (mm) max
1	II	-5	0.8 (0;3)	0.23	0.59
2	II		2 (0;3)	0.46	2.05
3	II		0.2 (0;1)	0.52	0.52
4	II		0.8 (0;2)	0.33	0.76
5	II	-15	2.2 (0;8)	0.09	1.00
6	II		3 (0;9)	0.12	1.07
7	II		2.4 (0;6)	0.16	0.68
8	II		2.4 (1;6)	0.27	2.93
9	GG	-7	0 (0;0)	–	–
10	GG		0.8 (0;2)	0.04	0.20
11	GG		1.3 (0;4)	0.02	0.24
12	GI		0.2 (0;1)	0.09	0.15
13	GI		0.9 (0;2)	0.02	1.12
14	GI		2.3 (0;4)	0.02	0.50
15	MC		1.51 (0;4)	0.07	0.38

tends to decrease as the particle density increases. This can be attributed to the fact that the particle's structural integrity and surface properties change with change in temperature at which they were generated. The higher density graupels generated at -7 °C are structurally more integrated (see Fig. 1a) than the ones produced at -15°C (Fig. 1b), thus reducing the chance of breaking and generating less fragments during collision. Certainly, ice pellets produce the least number of fragments due to their bulk structure.

The change in particle morphology can also be expressed in terms of the surface density A and fragility C of breakable asperities on the particle's surface (cf. Eq. 2). The surface property of the particles mainly determines the available number of breakable asperities on the surface. If a graupel has a lower density, i.e. more air bubble inclusions are formed when the particle was generated (Enzmann et al., 2011), it has more asperities than a higher density one. This is obvious also from Fig. 1; graupel generated at -15 °C has more roughness (crevices) on the surface and hence a greater number of breakable asperities than the relatively rather smooth graupel generated at -7 °C. Since the structure of a low-density particle is more loose and fluffy, those asperities are also more fragile, i.e. require less energy to break them off. Consequently, both parameters, A and C should increase by decreasing graupel density. This is reflected in Fig. 4 which shows the variation in A and C as a function of density calculated from the fit curves in Fig. 3. The lowest density particle in Fig. 4 is the graupel with dendrite in G2023, while the one with the highest density is the ice pellet. The parameters A and C together with their errors are given in Table 3.

https://doi.org/10.5194/egusphere-2024-3222
Preprint. Discussion started: 20 November 2024

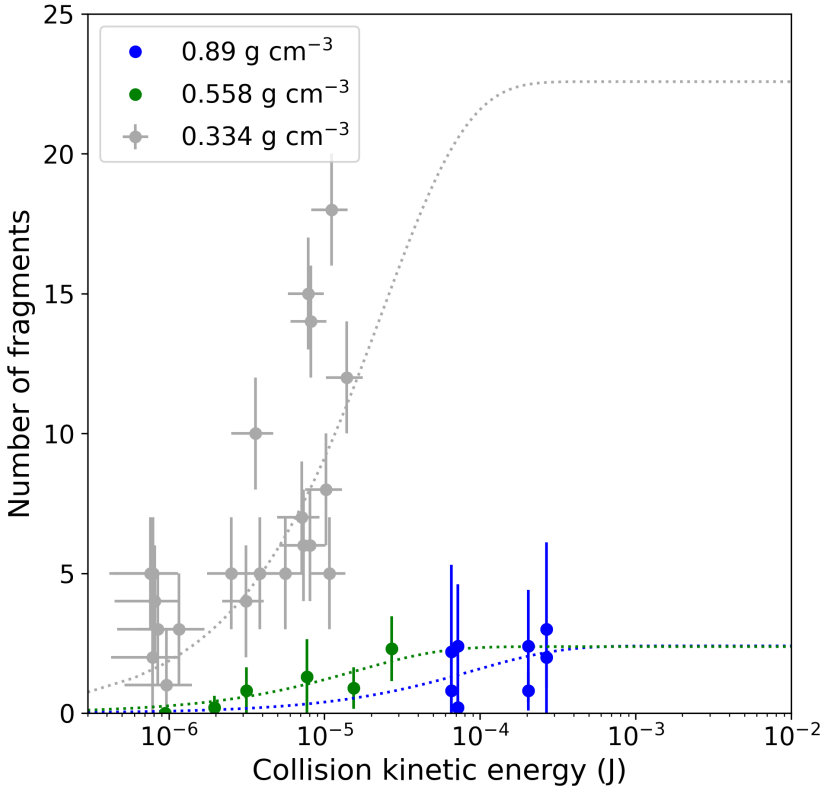

Figure 3. Number of fragments generated in bare graupel — bare graupel collisions. Blue: current study, ice pellet — ice pellet collisions (-5 and -15 °C); green: current study, graupel-graupel collisions (-7 °C); grey: G2023 bare graupel– bare graupel collisions (-15 °C). Dashed lines represent the best fits using Eq. 2.

Density (g/cm^3)	A (m^{-2})	ΔA (m^{-2})	C (J^{-1})	ΔC (J^{-1})
0.21	$4.68 \cdot 10^7$	$1.49 \cdot 10^6$	$1.10 \cdot 10^8$	$1.06 \cdot 10^7$
0.334	$1.27 \cdot 10^6$	$1.61 \cdot 10^5$	$1.57 \cdot 10^6$	228785
0.558	126168	19953	150597	55629
0.89	30610	9093	26534	20171

Table 3. Number density of breakable asperities, A, and the asperity-fragility coefficient, C, together with their errors from fits on our experimental data in Fig. 3 and G2023 for different particle densities.

In their theoretical framework, P2017 proposed the parameters A and C fitted to the experimental data of Takahashi et al. (1995). Following Table 1 of P2017 for Type I collisions, one can calculate $A = 6.8 \cdot 10^6$ to $18.6 \cdot 10^6$ m^{-2} depending on

https://doi.org/10.5194/egusphere-2024-3222
Preprint. Discussion started: 20 November 2024

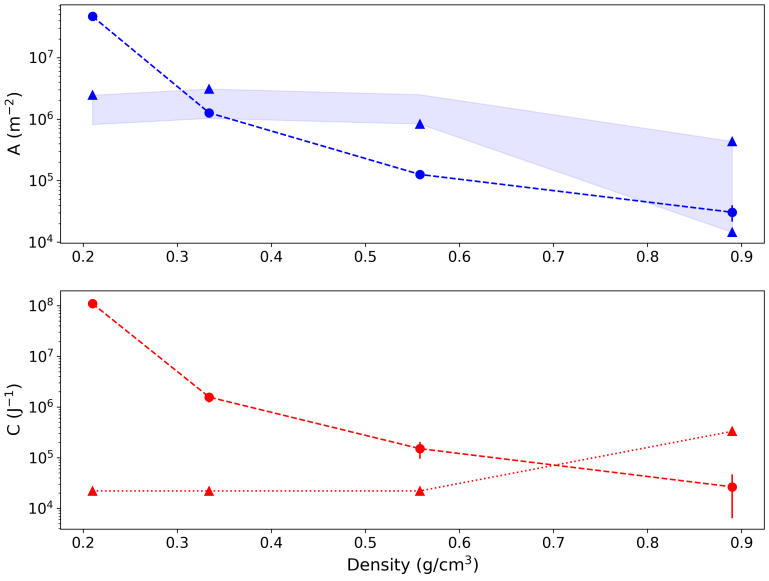

Figure 4. Experimentally determined surface density of breakable asperities A (upper panel, blue dots) and asperity-fragility coefficient C (lower panel, red dots) as a function of particle density. Blue and red triangles depict A and C using the Phillips et al. (2017) parameterization. The shaded area is corresponding to a temperature variation from -5 °C to -15 °C using the Phillips et al. (2017) parameterization.

graupel size and temperature, as well as $C = 22050$ J^{-1} and $C = 331000$ for graupel-graupel and ice pellet – ice pellet collisions, respectively. In the P2017 parameterization, both A and C are independent of the particle density. In contrast to these findings, we could demonstrate that A and C are dependent on the density of the colliding particles, thereby we refined and improved upon the previous parameterization.

One has to note here, that we did not carry out any systematic investigation upon the temperature dependency of the fragment numbers. The experiments of Takahashi et al. (1995) indicated a strong variation with temperature, which was also taken into account for in the parameterization of P2017. In agreement with Takahashi et al. (1995) and with P2017, in our opinion this temperature dependency can be attributed to the temperature dependency of the crystal habit, surface density, and size grown on the graupel's surface. For bare graupel and ice pellets such a strong temperature dependency is not expected, but some structural or morphological change is very likely.

The sizes of the graupels corresponding to the three lowest densities investigated in our study were approximately the same. Thus, the largest variation in the generated number of fragments, or in the parameters A and C stems from the temperature variation. In the P2017 parameterization, C is invariant on the temperature. Values of A were calculated for the particle sizes and temperature range of our experiments and indicated by the shaded area in Fig. 4. (Because we investigated ice pellets of

https://doi.org/10.5194/egusphere-2024-3222
Preprint. Discussion started: 20 November 2024

two different sizes, two triangles are shown in Fig. 4 at 0.89 g cm^{-3}.) Since this variation is far less then the observed change in A over the different particle types, one can attribute the systematic reduction of A indeed to the density of the particles.

In Fig. 4, A for ice pellets owns the lowest value both in our experiments and in the P2017 parameterization, having very good agreement at -5 °C. Nevertheless, the predicted temperature dependency of P2017 could not be proven in our measurements. As can be seen in Fig. 2a, the temperature dependency, if any, is within our experimental errors. As mentioned above, the temperature dependency in the P2017 parameterization might be attributed to the temperature dependency of the crystal growth on the ice sphere's surface. Since in our experiments solely the internal structure of the ice spheres can vary due to any temperature change, the resulted temperature dependency becomes minor.

The fragility coefficient C shows similar dependency on the particle density as A in our experiments, but behaves very differently to that of P2017 when employing their Type I parameterization corresponding to graupel-graupel or hail-hail collisions. Nevertheless, the P2017 parameterization was based on a very limited dataset available at that time which prevented the resolution of the full dependencies of C on temperature, size, and rimed fraction. Our experimental data shed light on the dependency of C at least on particle structure (i.e. rimed fraction) and probably temperature.

4.3 Multiple collision

In the multiple collision experiments, 2.45-mm-diameter graupels were repeatedly hit by 5-mm-diameter ice spheres until no more fragments were generated on their subsequent collisions. In these experiments, it took two to four collisions to cease generating any additional fragments. On an average 1.5 fragments, and a maximum of 4 fragments were released during these series of multiple collisions, which match the fragment numbers of single collisions (see Table 2). The number of released fragments was the highest for the very first collision in each set of measurements. The subsequent collisions did not show any clear tendency for decreasing or increasing number of fragments. Thus, apparently the majority of the breakable asperities broke at the very first collision, and none of them remained after the forth collision. The maximum fragment dimension was 0.384 mm and the minimum 0.072 mm, that also match the values for single collisions (Table 2). Hence, if a graupel suffers multiple collisions, it behaves like in single-collision events but it stops generating additional fragments after a few collisions. Nevertheless, if the graupel is in the mixed phase zone of a cloud, i.e. it can continuously grow by riming, its structure is retained in the sense that breakable asperities are continuously produced. Considering the relatively long time between two collision when compared to the growth rate by riming, single collision of graupels can be taken into account when considering secondary ice production.

5 Conclusions

Building upon the collision studies by G2023, we investigated the outcomes of collisions between graupel particles of different densities, specifically in the absence of fragile ice crystal growth on their surfaces. Collisions involving graupels grown at different temperatures by riming under dry growth conditions, and ice pellets generated as frozen water were investigated. Combining the dataset of the present study with those from G2023, in which the graupels had densities between approximately

https://doi.org/10.5194/egusphere-2024-3222
Preprint. Discussion started: 20 November 2024

0.2 and 0.34 g/cm^3, revealed a direct dependency of the number of fragments generated by collision on the particle's density. This effect can be attributed to the morphological structure of the particles, which ultimately determines both their fragility and their density. P2017 noted that the number of fragments generated increases with the degree of rime of graupels. This increase is explicable in terms of the number density of breakable branches, A, as also our study suggests. Our findings contradict the experimental study of Griggs and Choularton (1986) who suggested that fragmentation of rime is very unlikely to occur in natural clouds. Nevertheless, they pointed out that evaporation of rime in an unsaturated environment of the cloud would weaken the structure making the rimed graupel more fragile.

P2017 provided a temperature dependent parameterization of the number of fragments produced after collision. We haven't observed as high temperature dependency as P2017, however, the graupels' structure is determined by the temperature at which the growth occurs. Hence, one can argue that from this point of view our results also revealed an indirect temperature dependency. This suggests that the internal structural integrity of the particle varies with temperature, thereby altering its susceptibility to fracture. Nevertheless, the temperature dependency in P2017 might also be attributed to the temperature dependency of the crystal growth on the ice particle surface in the experiment of Takahashi et al. (1995).

The observed number of fragments produced by graupel- graupel collisions is within the range or higher than those observed in other secondary ice processes during drop freezing Lauber et al. (2018); Keinert et al. (2020). However, as showed in G2023 for graupel-snowflake and graupel-graupel with dendrites collisions, when ice particles posses vapor grown fragile ice structures, the number of ice fragments can rise up to hundred for one collision. The typical cloud regime range for collision induced fragmentation of ice pellets might coincide to that for fragmentation of freezing drops, whereas fragmentation of graupels would occur at lower cloud regimes and at temperatures between -5 °C and -20° C. This regime falls within the typical H-M range, however, the observed number of fragments is far less than those suggested from H-M processes. Therefore, we suggest sensitivity studies using cloud models to explore the role of collision induced fragmentation of graupels in the H-M regime in ice multiplication and cloud and precipitation development.

Data availability. The data set used for generating the figures is available at https://doi.org/10.5281/zenodo.14140846 (Yadav et al., 2024) and https://doi.org/10.5281/zenodo.8348271 (Grzegorczyk et al., 2023a). The raw measurement data will be provided upon request.

Author contributions. The paper was written by M.S. and S. Y. with the support and assistance of all co-authors; P.G. made significant contributions by providing comments on the results, discussion, and conclusion, as well as in data evaluation; S.Y. performed graupel growth and collision experiments, and evaluated the data; L.M. performed ice pellets experiments and analyzed the data; A.T. constructed the graupel generator, designed the graupel growth experiments; S.K.M. and S.Y. designed the graupel growth and collision experiments and characterized the setups; M.S. designed the experiments, analyzed the data.

Competing interests. The authors declare no competing interest.

https://doi.org/10.5194/egusphere-2024-3222
Preprint. Discussion started: 20 November 2024

Acknowledgements. We gratefully acknowledge the funding of the German Research Foundation (DFG) to initialize the special priority programme on the Fusion of Radar Polarimetry and Atmospheric Modelling (SPP-2115, PROM). The work of contributing authors was carried out in the framework of the project "FRAGILE: Exploring the role of FRAGmentation of ice particles by combining super-partIcle modelling, Laborotary studies, and polarimEtric radar observations" (Grant KN 1112/5). We also gratefully acknowledge the help of Dr. Christoph Sievert (German Weather Service) in the calculation of the collision kinetic energy of atmospheric graupels and ice pellets.

https://doi.org/10.5194/egusphere-2024-3222
Preprint. Discussion started: 20 November 2024

References

Choularton, T., Latham, J., and Mason, B. J.: A possible mechanism of ice splinter production during riming, Nature, 274, 791–792, 1978.

Choularton, T. W., Griggs, D. J., Humood, B. Y., and Latham, J.: Laboratory studies of riming, and its relation to ice splinter production, Quarterly Journal of the Royal Meteorological Society, 106, 367–374, https://doi.org/10.1002/qj.49710644809, 1980.

Enzmann, F., Miedaner, M. M., Kersten, M., von Blohn, N., Diehl, K., Borrmann, S., Stampanoni, M., Ammann, M., and Huthwelker, T.: 3-D imaging and quantification of graupel porosity by synchrotron-based micro-tomography, Atmospheric Measurement Techniques, 4, 2225–2234, https://doi.org/10.5194/amt-4-2225-2011, 2011.

Field, P. R., Lawson, R. P., Brown, P. R. A., Lloyd, G., Westbrook, C., Moisseev, D., Miltenberger, A., Nenes, A., Blyth, A., Choularton, T., Connolly, P., Buehl, J., Crosier, J., Cui, Z., Dearden, C., DeMott, P., Flossmann, A., Heymsfield, A., Huang, Y., Kalesse, H., Kanji, Z. A., Korolev, A., Kirchgaessner, A., Lasher-Trapp, S., Leisner, T., McFarquhar, G., Phillips, V., Stith, J., and Sullivan, S.: Chapter 7. Secondary Ice Production - current state of the science and recommendations for the future, Meteorological Monographs, https://doi.org/10.1175/amsmonographs-d-16-0014.1, 2017.

Griggs, D. J. and Choularton, T. W.: A laboratory study of secondary ice particle production by the fragmentation of rime and vapour-grown ice crystals, Quarterly Journal of the Royal Meteorological Society, 112, 149–163, https://doi.org/10.1002/qj.49711247109, 1986.

Grzegorczyk, P., Yadav, S., Zander, F., Theis, A., Mitra, S. K., and Szakáll, M.: Experimental data for "Fragmentation of ice particles: laboratory experiments on graupel- graupel and graupel-snowflake collisions", https://doi.org/10.5281/zenodo.8348271, 2023a.

Grzegorczyk, P., Yadav, S., Zanger, F., Theis, A., Mitra, S. K., Borrmann, S., and Szakáll, M.: Fragmentation of ice particles: laboratory experiments on graupel–graupel and graupel–snowflake collisions, Atmospheric Chemistry and Physics, 23, 13 505–13 521, https://doi.org/10.5194/acp-23-13505-2023, 2023b.

Hallett, J. and Mossop, S. C.: Production of secondary ice particles during the riming process, Nature, 249, 26–28, https://doi.org/10.1038/249026a0, 1974.

Heymsfield, A., Szakáll, M., Jost, A., Giammanco, I., Wright, R., and Brimelow, J.: CORRIGENDUM, Journal of the Atmospheric Sciences, 77, 405 – 412, https://doi.org/10.1175/JAS-D-19-0185.1, 2020.

Heymsfield, A. J. and Mossop, S. C.: Temperature dependence of secondary ice crystal production during soft hail growth by riming, Quarterly Journal of the Royal Meteorological Society, 110, 765–770, https://doi.org/10.1002/qj.49711046512, 1984.

James, R. L., Phillips, V. T. J., and Connolly, P. J.: Secondary ice production during the break-up of freezing water drops on impact with ice particles, Atmospheric Chemistry and Physics, 21, 18 519–18 530, https://doi.org/10.5194/acp-21-18519-2021, 2021.

Keinert, A., Spannagel, D., Leisner, T., and Kiselev, A.: Secondary Ice Production upon Freezing of Freely Falling Drizzle Droplets, Journal of the Atmospheric Sciences, 77, 2959 – 2967, https://doi.org/10.1175/JAS-D-20-0081.1, 2020.

Korolev, A. and Leisner, T.: Review of experimental studies of secondary ice production, Atmospheric Chemistry and Physics, 20, 11 767–11 797, https://doi.org/10.5194/acp-20-11767-2020, 2020.

Korolev, A., DeMott, P. J., Heckman, I., Wolde, M., Williams, E., Smalley, D. J., and Donovan, M. F.: Observation of secondary ice production in clouds at low temperatures, Atmospheric Chemistry and Physics, 22, 13 103–13 113, https://doi.org/10.5194/acp-22-13103-2022, 2022.

Lachapelle, M. and Thériault, J. M.: Characteristics of Precipitation Particles and Microphysical Processes during the 11–12 January 2020 Ice Pellet Storm in the Montréal Area, Québec, Canada, Monthly Weather Review, 150, 1043 – 1059, https://doi.org/10.1175/MWR-D-21-0185.1, 2022.

https://doi.org/10.5194/egusphere-2024-3222
Preprint. Discussion started: 20 November 2024

Lauber, A., Kiselev, A., Pander, T., Handmann, P., and Leisner, T.: Secondary Ice Formation during Freezing of Levitated Droplets, Journal of the Atmospheric Sciences, 75, 2815 – 2826, https://doi.org/10.1175/JAS-D-18-0052.1, 2018.

Mossop, S. C.: Production of secondary ice particles during the growth of graupel by riming, Quarterly Journal of the Royal Meteorological Society, 102, 45–57, https://doi.org/10.1002/qj.49710243104, 1976.

Phillips, V. T. J., Yano, J.-I., and Khain, A.: Ice Multiplication by Breakup in Ice–Ice Collisions. Part I: Theoretical Formulation, Journal of the Atmospheric Sciences, 74, 1705–1719, https://doi.org/10.1175/JAS-D-16-0224.1, 2017.

Seidel, J. S., Kiselev, A. A., Keinert, A., Stratmann, F., Leisner, T., and Hartmann, S.: Secondary ice production – no evidence of efficient rime-splintering mechanism, Atmospheric Chemistry and Physics, 24, 5247–5263, https://doi.org/10.5194/acp-24-5247-2024, 2024.

Takahashi, T., Nagao, Y., and Kushiyama, Y.: Possible High Ice Particle Production during Graupel–Graupel Collisions, Journal of the Atmospheric Sciences, 52, 4523–4527, https://doi.org/10.1175/1520-0469(1995)052<4523:phippd>2.0.co;2, 1995.

Theis, A., Szakáll, M., Diehl, K., Mitra, S. K., Zanger, F., Heymsfield, A., and Borrmann, S.: Vertical Wind Tunnel Experiments and a Theoretical Study on the Microphysics of Melting Low-Density Graupel, Journal of the Atmospheric Sciences, 79, 1069–1087, https://doi.org/10.1175/jas-d-21-0162.1, 2022.

Tridon, F., Silber, I., Battaglia, A., Kneifel, S., Fridlind, A., Kalogeras, P., and Dhillon, R.: Highly supercooled riming and unusual triple-frequency radar signatures over McMurdo Station, Antarctica, Atmospheric Chemistry and Physics, 22, 12 467–12 491, https://doi.org/10.5194/acp-22-12467-2022, 2022.

Vardiman, L.: The Generation of Secondary Ice Particles in Clouds by Crystal–Crystal Collision, Journal of the Atmospheric Sciences, 35, 2168–2180, https://doi.org/10.1175/1520-0469(1978)035<2168:tgosip>2.0.co;2, 1978.

von Terzi, L., Dias Neto, J., Ori, D., Myagkov, A., and Kneifel, S.: Ice microphysical processes in the dendritic growth layer: a statistical analysis combining multi-frequency and polarimetric Doppler cloud radar observations, Atmospheric Chemistry and Physics, 22, 11 795–11 821, https://doi.org/10.5194/acp-22-11795-2022, 2022.

Waitz, F., Schnaiter, M., Leisner, T., and Järvinen, E.: In situ observation of riming in mixed-phase clouds using the PHIPS probe, Atmospheric Chemistry and Physics, 22, 7087–7103, https://doi.org/10.5194/acp-22-7087-2022, 2022.

Yadav, S., Metten, L., Grzegorczyk, P., Theis, A., Mitra, S. K., and Szakáll, M.: Experimental data for "Measurement Report: Influence of particle density on secondary ice production by graupel and ice pellet collisions", https://doi.org/10.5281/zenodo.14140846, 2024.